PCCP

PAPER

View Article Online
View Journal | View Issue

Cite this: *Phys. Chem. Chem. Phys.*, 2014, **16**, 18736

Interfacial reactivity of ruthenium nanoparticles protected by ferrocenecarboxylates†

Limei Chen,[a] Yang Song,[a] Peiguang Hu,[a] Christopher P. Deming,[a] Yan Guo[ab] and Shaowei Chen*[a]

Received 2nd May 2014,
Accepted 21st July 2014

DOI: 10.1039/c4cp01890g

www.rsc.org/pccp

Stable ruthenium nanoparticles protected by ferrocenecarboxylates (RuFCA) were synthesized by thermolytic reduction of $RuCl_3$ in 1,2-propanediol. The resulting particles exhibited an average core diameter of 1.22 ± 0.23 nm, as determined by TEM measurements. FTIR and ^{1}H NMR spectroscopic measurements showed that the ligands were bound onto the nanoparticle surface *via* Ru–O bonds in a bidentate configuration. XPS measurements exhibited a rather apparent positive shift of the Fe2p binding energy when the ligands were bound on the nanoparticle surface, which was ascribed to the formation of highly polarized Ru–O interfacial bonds that diminished the electron density of the iron centers. Consistent results were obtained in electrochemical measurements where the formal potential of the nanoparticle-bound ferrocenyl moieties was found to increase by *ca.* 120 mV. Interestingly, galvanic exchange reactions of the RuFCA nanoparticles with Pd(II) followed by hydrothermal treatment at 200 °C led to (partial) decarboxylation of the ligands such that the ferrocenyl moieties were now directly bonded to the metal surface, as manifested in voltammetric measurements that suggested intervalence charge transfer between the nanoparticle-bound ferrocene groups.

Introduction

Monolayer-protected metal nanoparticles have attracted great interest in diverse research fields such as catalysis,[1] energy conversion and storage,[2] biological and chemical sensing,[3] *etc.* In these studies, metal–ligand bonding interactions have been found to play a key role in the determination of the nanoparticle size, structure, stability, and reactivity.[4] Whereas mercapto derivatives have been used extensively as the ligands of choice for nanoparticle surface functionalization because of the strong affinity of the thiol moiety to metal surfaces, recently a number of studies have been carried out focusing on the synthesis of metal nanoparticles stabilized by other metal–ligand interfacial bonds. With the new interfacial chemistry, not only the growth dynamics of the nanoparticles changes accordingly, but more interestingly the nanoparticle optical and electronic properties can also be manipulated at an unprecedented level as a result of the unique bonding interactions between the metal cores and the organic capping ligands. For instance, alkylamines have been used as capping ligands in the control of the size and shape of ruthenium nanoparticles because of their strong coordination bonds. Experimentally it has been observed that the ruthenium particles tend to be elongated or form rod-like structures thanks to the fast exchange of amine ligands at the particle surface.[5] However, in the presence of ionic liquids (*e.g.*, imidazolium-derived ionic liquids), spherical nanoparticles are obtained as ligand exchange is inhibited.[6] Stable metal nanoparticles have also been prepared by taking advantage of the self-assembly of diazo and acetylene derivatives onto metal nanoparticle surfaces forming metal–carbene (M=C), –acetylide (M–C≡), or –vinylidene (M=C=C) π bonds.[7–11] With the formation of these conjugated interfacial bonds, extensive intraparticle charge delocalization occurs between the particle-bound functional moieties, leading to the emergence of optical and electronic properties that are analogous to those of their dimeric derivatives.[12–15]

In these studies, ruthenium nanoparticles have been used rather extensively as the illustrating examples, possibly because of the rich chemistry manifested in relevant ruthenium complexes.[16] Among the methods for the synthesis of ruthenium nanoparticles, thermolysis is an effective route where Ru(III) precursors are reduced in alcohols in the presence of acetate salts.[17] The resulting ruthenium colloids are presumed to be stabilized by the acetate ligands, which may be replaced by ligand exchange with thiols or alkyne ligands.[9] However, other carboxylate derivatives have rarely been used,[2,18] and few studies have focused on the interfacial interactions between

[a] *Department of Chemistry and Biochemistry, University of California, 1156 High Street, Santa Cruz, California 95064, USA. E-mail: shaowei@ucsc.edu*
[b] *School of Environmental Science and Engineering, Nanjing University of Information Science & Technology, Nanjing, Jiangsu 210044, P. R. China*

† Electronic supplementary information (ESI) available: Additional TEM and spectroscopic data of the nanoparticle samples. See DOI: 10.1039/c4cp01890g

the metal cores and the carboxylate groups. This is the primary motivation of the present study.

Herein, we used sodium ferrocenecarboxylate as a new type of protecting ligands for the stabilization of ruthenium nanoparticles by the formation of Ru–O interfacial bonds, where the ferrocenyl groups were exploited as a molecular probe to examine the nanoparticle interfacial reactivity. Interestingly, sodium ferrocenecarboxylate was found to act as a better stabilizer than sodium acetate for ruthenium nanoparticles. The resulting nanoparticles were then subject to detailed characterizations by a wide array of spectroscopic and microscopic measurements, including transmission electron microscopy (TEM), ^{1}H nuclear magnetic resonance (NMR) spectroscopy, ultraviolet-visible (UV-vis) absorption, as well as Fourier-transformed infrared (FTIR) spectroscopy. The ligands were found to form highly polarized Ru–O bonds at the metal–ligand interface in a bidentate configuration,[19] in consistence with X-ray photoelectron spectroscopic (XPS) measurements which exhibited a marked increase of the Fe2p binding energy and electrochemical measurements where the formal potential of the particle-bound ferrocenyl moieties increased by *ca.* 120 mV. Notably, the nanoparticles might undergo galvanic exchange reactions with Pd(II), and after hydrothermal reactions, the resulting nanoparticles exhibited voltammetric results that suggested intervalence charge transfer between the ferrocenyl groups on the nanoparticle surface, likely because of palladium-catalyzed decarboxylation of the surface ligands and the ferrocenyl groups were now directly bonded to the metal surfaces.

Experimental section

Chemicals

Ruthenium chloride ($RuCl_3$, 35–40% Ru, ACROS), sodium hydroxide (NaOH, extra pure, ACROS), 1,2-propanediol (ACROS), palladium(II) chloride ($PdCl_2$, 59% Pd, ACROS), hydrochloric acid (HCl, ACS Reagent, Sigma-Aldrich) and ferrocenecarboxylic acid (FCA, 98+%, Santa Cruz Biotechnology) were used as received. All solvents were obtained from typical commercial sources and used without further treatment. Water was supplied by a Barnstead Nanopure water system (18.3 MΩ cm).

Preparation of ferrocenecarboxylate-stabilized ruthenium nanoparticles

Ferrocenecarboxylate-stabilized Ru nanoparticles were synthesized by thermolytic reduction of $RuCl_3$ in 1,2-propanediol, similar to the preparation of acetate-stabilized Ru colloids described in previous studies.[7] Briefly, 0.1 mmol of $RuCl_3$, 0.6 mmol of FCA and 0.6 mmol of sodium hydroxide were dissolved in 100 mL of 1,2-propanediol. The solution was then heated to 175 °C for 2 h under vigorous stirring. During the reaction, the color of the solution was found to change from dark orange to dark brown indicating the formation of Ru nanoparticles. The colloid solution was then cooled to room temperature and underwent dialysis for 3 d in nanopure water to remove excessive ligands of FCA and 1,2-propanediol. The solution was then collected and dried by rotary evaporation, and the solids were rinsed extensively with acetonitrile to remove residual free ligands. The resulting purified ruthenium nanoparticles were denoted as RuFCA.

Decarboxylation of RuFCA nanoparticles

The experimental procedure is depicted in Scheme 1. A H_2PdCl_4 solution was first prepared by dissolving $PdCl_2$ (0.1 mmol) in hydrochloric acid (1 mL) at 50 °C. When cooled down to room temperature, the solution was added to the RuFCA nanoparticle solution in 1,3-propanediol for galvanic exchange. After magnetic stirring for 24 h, the solution was purified by dialysis in nanopure water and rinsing by acetonitrile to remove excessive free ligands and reaction by-products. The solution was then added into a Teflon-lined autoclave, which was sealed and placed in an oven and heated at 200 °C for 4 h. The precipitates were collected and purified by rinsing extensively with acetonitrile; and the resulting nanoparticles were referred to as RuPdFCA.

Characterizations

The particles core diameters were determined by TEM measurements with a JEOL-F 200 KV field-emission analytical transmission electron microscope. The samples were prepared by casting a drop of the particle solution in *N*,*N*-dimethylformamide (DMF) onto a 200 mesh holey carbon-coated copper grid. ^{1}H NMR spectroscopic measurements were carried out by

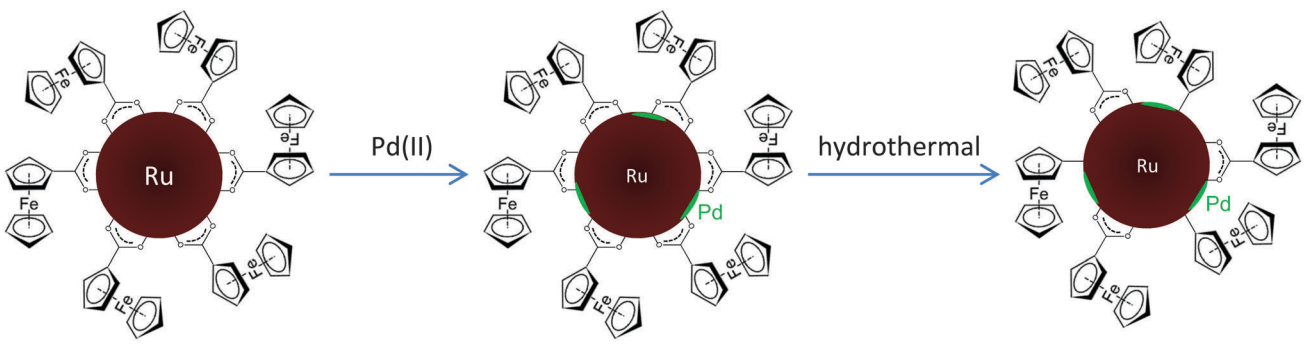

Scheme 1

using concentrated solutions of the nanoparticles in deuterated DMF with a Varian UnityPlus 500 MHz NMR spectrometer and the absence of any sharp features indicated that the nanoparticles were free of excessive monomeric ligands. UV-vis spectroscopic studies were performed with an ATI Unicam UV4 spectrometer using a 10 mm quartz cuvette with a resolution of 2 nm. FTIR measurements were carried out with a Perkin-Elmer FTIR spectrometer (Spectrum One, spectral resolution 4 cm^{-1}), where the samples were prepared by casting the particle solutions onto a ZnSe disk. X-Ray photoelectron spectra (XPS) were recorded with a PHI 5400/XPS instrument equipped with an Al Kα source operated at 350 W and at 10^{-9} Torr. Silicon wafers were sputtered by argon ions to remove carbon from the background and used as substrates. The spectra were charge-referenced to the Si2p peak (99.3 eV).

Electrochemistry

Voltammetric measurements were carried out with a CHI 440 electrochemical workstation. A polycrystalline gold disk electrode (sealed in glass tubing) was used as the working electrode, with a surface area of 0.70 mm^2. A Ag/AgCl wire and a Pt coil were used as the (quasi)reference and counter electrodes, respectively. The gold electrode was first polished with 0.05 μm alumina slurries and then cleansed by sonication in H_2SO_4 and nanopure water successively. Note that the potentials were all calibrated against the formal potential of ferrocene monomers (Fc^+/Fc) in the same electrolyte solution.

Results and discussion

Fig. 1 depicts a representative TEM micrograph of the RuFCA nanoparticles. It can be seen that the nanoparticles were well dispersed without apparent aggregation, suggesting effective stabilization of the nanoparticles by the ferrocenecarboxylate ligands. Statistical analysis based on more than 100 nanoparticles showed that the nanoparticles were largely within the narrow range of 0.80 to 1.70 nm in diameter, with a mean value of 1.22 ± 0.23 nm, as manifested in the figure inset.

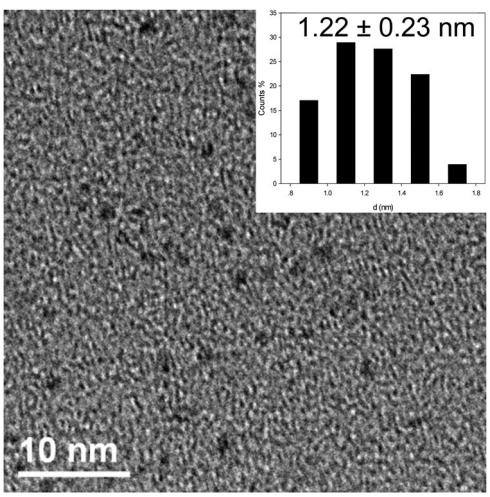

Fig. 1 Representative TEM micrograph of RuFCA nanoparticles. The inset shows the particle core size histogram. The scale bar is 10 nm.

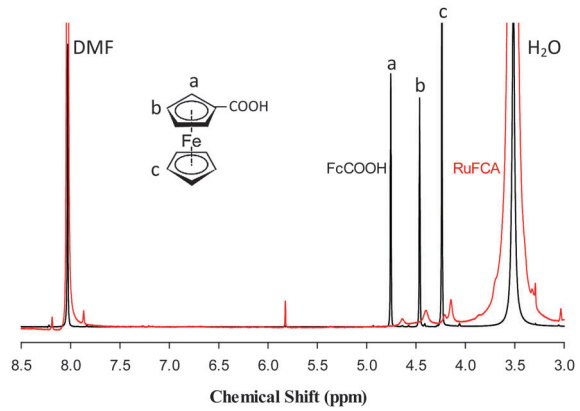

Fig. 2 ^{1}H NMR spectra of (black curve) monomeric FCA and (red curve) RuFCA nanoparticles in deuterated DMF.

The structures of the RuFCA nanoparticles were then examined by NMR measurements. Fig. 2 shows the ^{1}H NMR spectra of RuFCA and monomeric FCA in deuterated DMF. For the monomeric FCA ligands (black curve), three sharp multiplets can be identified at 4.75, 4.46 and 4.24 ppm with the ratio of the integrated peak areas at about a : b : c = 1.08 : 1 : 2.59. These are consistent with those of the ferrocenyl ring protons as depicted in the figure inset (the peak at *ca.* 8.0 ppm was from the DMF solvent and that at 3.5 ppm was due to residual water in the solvent). For the RuFCA nanoparticles (red curve), however, these three peaks were found to shift somewhat to 4.66, 4.40, and 4.20 ppm, which suggests decreasing electron density (bonding order) of the ferrocenyl skeleton (*vide infra*) as compared to that of the monomeric ligands. In addition, the peaks were apparently broadened and the ratio of the integrated peak areas reduced to a : b : c = 0.37 : 1 : 1.72. The broadening can be attributed to inhomogeneity of the magnetic field in the local chemical environments on the ruthenium nanoparticle surface.[20] The closer the protons are to the metal cores, the stronger the influence is. Thus the deviation of the ratio of the (a), (b) and (c) protons from the expected value of 1 : 1 : 2.5 is most likely due to the varied degrees of signal broadening. In particular, the apparent underestimation of protons (a) may be accounted for by their close proximity to the carboxylic acid moieties that are the presumed anchoring sites onto the nanoparticle surface. Furthermore, the lack of sharp features in the NMR measurements indicates that the nanoparticles were free of excessive monomeric ligands. Such a phenomenon has been observed extensively with organically capped metal nanoparticles, as a result of (1) spin relaxation from dipolar interactions at the ligand/core interface and (2) spin–spin relaxation broadening caused by particle core size dispersity.[7]

FTIR measurements further confirmed that the FCA ligands were indeed bound on the nanoparticle surface with the carboxylate moieties symmetrically anchored to Ru, as depicted in Fig. 3. For the FCA monomers (black curve), the peaks at 1654 cm^{-1} and 1284 cm^{-1} may be assigned to the C=O

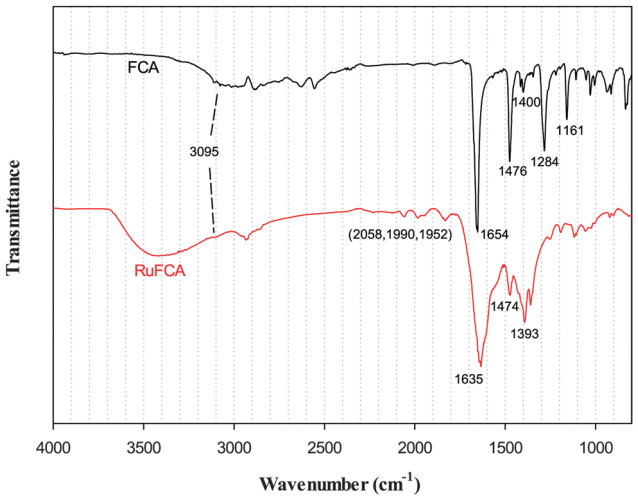

Fig. 3 FTIR spectra of FCA monomers (black curve) and RuFCA nanoparticles (red curve).

and C–O stretching vibrations of the carboxyl moieties, respectively; the ferrocenyl ring skeleton (C═C) vibrations can be found at 1476 and 1400 cm^{-1}, along with the cyclopentadienyl C–H vibrational stretch at about 3095 cm^{-1} and bending vibration at 1161 cm^{-1}.[21–23] Interestingly, when the ligands were bound onto the ruthenium nanoparticle surface (red curve), the C–O vibration peaks diminished significantly and the C═O band red-shifted to 1635 cm^{-1}. This decrease of bonding order might be accounted for by the formation of carboxylate-like species when the ligands were bound onto the nanoparticle surface in a bidentate configuration (Scheme 1), because of the strong coupling between C═O and C–O.[2,18] In addition, the ring skeleton vibrations of the ferrocenyl moieties red-shift slightly to 1474 and 1393 cm^{-1}. This is consistent with the red-shift of the ferrocenyl ring protons in NMR measurements as observed in Fig. 2. Additionally, one may notice that three small peaks emerged in the region of 1900 to 2100 cm^{-1}. These are likely due to Ru–H vibrational stretches that were formed in the thermolytic synthesis of ruthenium nanoparticles, where the variation of the vibrational frequencies might be ascribed to the Ru–H bonds at different surface sites.[24–26]

Further structural insights were obtained in XPS measurements. From the XPS survey spectra in Fig. 4(A), the elements of C (Ru), O and Fe can be clearly identified in both FCA monomers and RuFCA nanoparticles (note that the binding energy of C1s and Ru3d electrons overlaps around 285 eV[27]). Yet clear discrepancy can be seen in high-resolution scans, as manifested in panels (B) to (D) (black curves are experimental data and color curves are deconvolution fits). For instance, in panel (B), deconvolution of the XPS profile of the FCA monomers revealed two peaks at 285.7 (blue curve) and 288.8 eV (yellow curve), which may be assigned to the ferrocenyl (C═C) and

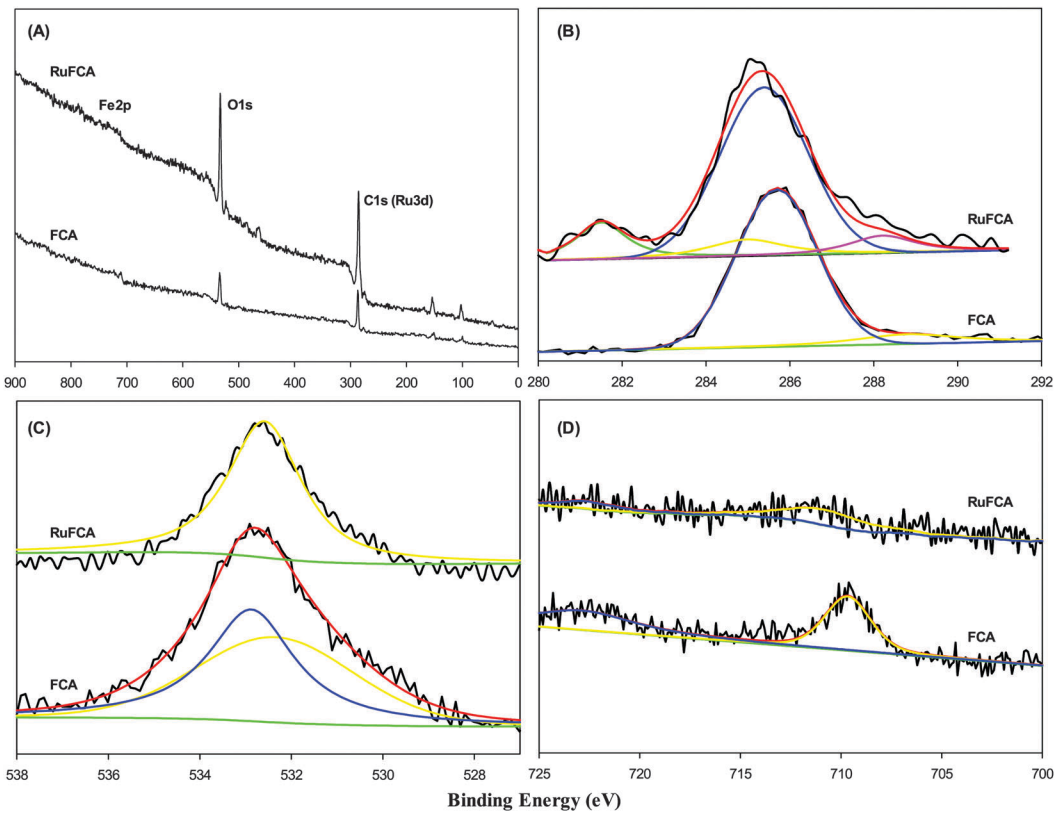

Fig. 4 (A) XPS survey spectra of FCA monomers, and RuFCA nanoparticles. High-resolution scans of the (B) C1s (Ru3d), (C) O1s and (D) Fe2p electrons are also included, where black curves are the experimental data and color curves are the corresponding deconvolution fits.

carboxyl (COO) C1s, respectively; and the ratio of the integrated peak areas is estimated to be 9.3 : 1, close to 10 : 1 expected from the molecular structure. For the RuFCA nanoparticles, four peaks were resolved by deconvolution. Among these the one at 285.4 eV was most likely due to the ferrocenyl ring carbons (blue curve), the one at 287.6 eV to carbonyl carbon (magenta curve)—the ratio of their integrated peak areas is also close to 10 : 1, consistent with the bidentated binding of the FCA ligands onto the ruthenium nanoparticle surface (Scheme 1). Additionally, the pairs at 281.5 (green curve) and 285.6 eV (yellow curve) may be assigned to Ru3d electrons. It should be noted that in a previous study with alkyne-stabilized ruthenium nanoparticles, the binding energy of the Ru3d electron was found to be markedly lower at 280.5 and 284.6 eV.[27] This may be ascribed to the difference of the chemical nature of the metal–ligand interfacial bonds: in the present study, the attachment of carboxyl moieties onto the ruthenium nanoparticle surface led to the formation of highly polarized Ru–O bonds where charge transfer from Ru to O likely occurred, whereas in alkyne-stabilized nanoparticles, the ruthenium–vinylidene bonds were mostly covalent in nature.[27] The (partial) interfacial charge transfer in Ru–O might also account for the small red-shift of the binding energy of both the carboxyl and ferrocenyl C1s electrons in RuFCA nanoparticles, as compared to those of FCA monomers.

Consistent results were observed in the measurements of the O1s and Fe2p electrons. As shown in panel (C), for the FCA monomers, two peaks were resolved in the O1s spectrum at 532.4 (yellow curve) and 532.9 eV (blue curve), corresponding to the C═O and C–O oxygen, respectively. In contrast, only one peak is needed to fit the data of RuFCA which is centered at 532.6 eV, suggesting that the bonding order involved was in the intermediate between C═O and C–O. This is consistent with the structural configuration where the carboxyl moieties were bound onto the ruthenium nanoparticle surface in a symmetrical bidentate fashion (Scheme 1). Similarly, for Fe2p electrons that are shown in panel (D), it can be seen that for the FCA monomers, the Fe(II)2p electrons are well-defined at 709.7 eV (yellow curve) and 722.8 eV (blue curve), whereas 710.8 eV (yellow curve) and 722.6 eV (blue curve) for the RuFCA nanoparticles. This observation is likely due to the strong polarization of the Ru–O interfacial bonds that diminishes the electron density of the iron centers in RuFCA, in good agreement with the NMR and FTIR results presented above.[28]

The impacts of surface functionalization by ferrocenecarboxylate on the particle electronic properties were then examined by electrochemical measurements. Fig. 5 shows the square wave voltammograms (SWV) of the FCA monomers and RuFCA nanoparticles in DMF with 0.1 M tetra-*n*-butylammonium perchlorate (TBAP) as the supporting electrolyte at a gold disk electrode. The FCA monomers (black curves) exhibited one pair of voltammetric peaks within the potential range of −0.20 to +0.30 V, with the formal potential ($E^{o\prime}$) at +0.05 V *vs.* Fc^+/Fc. Similar voltammetric features can be seen with the RuFCA nanoparticles (red curves), with a rather comparable peak width at half maximum (103 mV and 110 mV for FCA and RuFCA, respectively); however

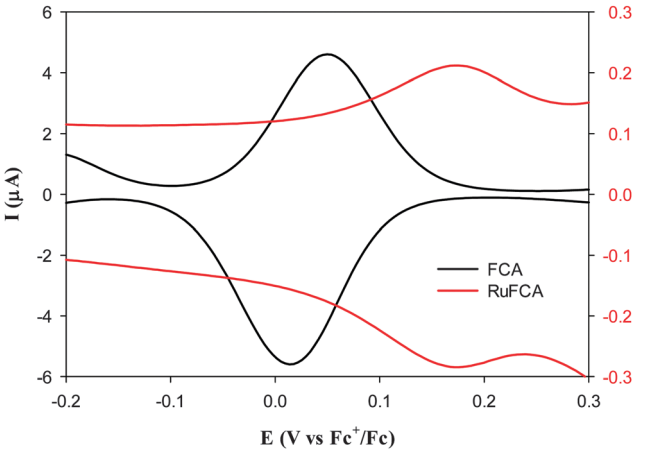

Fig. 5 SWVs of FCA monomers and RuFCA nanoparticles acquired at a gold electrode in 0.1 M tetrabutylammonium perchlorate (TBAP) in DMF. Electrode surface area 0.70 mm^2, FCA concentration 4.3 mM, RuFCA nanoparticle concentration 5 mg mL^{-1}, increment of potential 4 mV, amplitude 25 mV and frequency 15 Hz.

the formal potential was found to shift to +0.17 V, 120 mV more positive than that of FCA monomers. This is consistent with the above XPS results where the binding energy of the Fe2p electrons of the RuFCA nanoparticles was markedly higher than that of FCA monomers, again, because of the highly polarized Ru–O interfacial bonds that diminished the electron density of the iron centers (Scheme 1).

Interestingly, when the RuFCA nanoparticles underwent galvanic exchange reactions with $PdCl_4^{2-}$ followed by hydrothermal treatment at 200 °C for 4 h, the resulting nanoparticles exhibited drastically different voltammetric responses. This is to take advantage of the spontaneous galvanic exchange reaction of Ru(0) with Pd(II), as the redox potential of $PdCl_4^{2-}$ + 2e → Pd + $4Cl^-$ (+0.591 V *vs.* NHE) is more positive than that of Ru^{2+} + 2e → Ru (+0.455 V *vs.* NHE),[29] where Pd was most likely deposited on the nanoparticle surface in the form of small clusters (*vide infra*). It should be noted that Pd may serve as an effective catalyst for decarboxylation under hydrothermal conditions.[30] Therefore, the resulting RuPdFCA nanoparticles were subject to hydrothermal treatment. It was anticipated that the ferrocenyl moieties would be directly bonded to the metal cores (Scheme 1) such that intraparticle charge delocalization occurred between the particle-bound ferrocenyl groups. Indeed, as evidenced by the black curves in Fig. 6, electrochemical measurements of these nanoparticles exhibited two pairs of voltammetric peaks within the potential range of −0.30 to +0.40 V (*vs.* Fc^+/Fc), with the formal potentials at +0.190 and −0.072 V, a behavior consistent with intervalence charge transfer between the particle-bound ferrocenyl moieties.[8] Notably, the potential spacing (ΔV) of 260 mV between the two voltammetric peaks is markedly greater than those observed in the previous study (*ca.* 200 mV) where the ferrocenyl moieties were bound onto the ruthenium nanoparticles by ruthenium–carbene π bonds,[8] but very comparable to those of conventional biferrocene derivatives.[31,32] This is consistent with Class II compounds

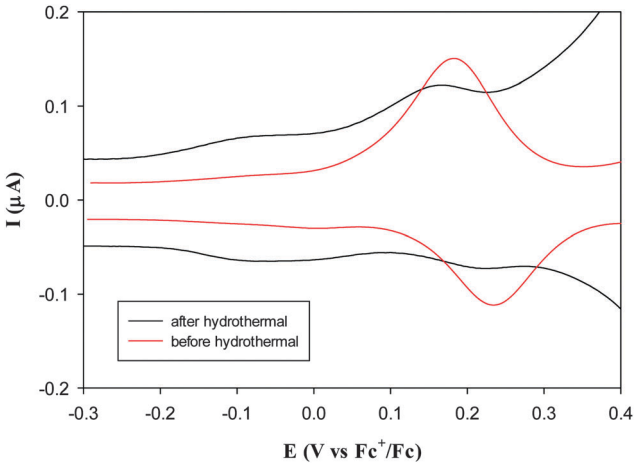

Fig. 6 SWVs of RuFCA nanoparticles after galvanic exchange reactions with Pd(II) followed by hydrothermal treatment at 200 °C for 4 h. Other experimental conditions the same as those in Fig. 5.

as defined by Robin and Day.[33] In sharp contrast, for the nanoparticles prior to hydrothermal treatment (red curves), only a single pair of voltammetric peaks appear at +0.20 V, indicating the lack of effective electronic communication between the ferrocenyl functional groups on the nanoparticle surface because of insulation by the Ru–O linkages.

Furthermore, there are several aspects that warrant attention here. First, the RuPdFCA nanoparticles exhibited almost unchanged UV-vis absorption profiles before and after hydrothermal treatments, which were also consistent with that of the original RuFCA nanoparticles (Fig. S1, ESI†), whereas TEM measurements showed that the size of the RuPdFCA nanoparticles increased to about 2.5 nm after hydrothermal treatments (Fig. S2, ESI†). Second, in FTIR measurements the C═O vibrational band at *ca.* 1639 cm^{-1} remained rather prominent with the hydrothermally treated RuPdFCA nanoparticles (Fig. S3, ESI†), suggesting incomplete decarboxylation of the FCA ligands on the nanoparticles. This is most likely due to the inhomogeneous distribution of the Pd (cluster) catalysts during galvanic exchange reactions and consistent with results from XPS measurements. From Fig. S4 (ESI†), in the full survey spectrum of the RuPdFCA nanoparticles the Pd3d electrons can be identified at around 340 eV. However the signals are rather weak, signifying a low Pd concentration (most likely in the form of small clusters) in the nanoparticles; and the low signals renders it difficult to have a reliable quantitative assessment of the Pd loading. In addition, deconvolution of the C1s and Ru3d region yields four peaks at 281.1 eV ($Ru3d_{5/2}$), 285.3 eV ($Ru3d_{3/2}$), 285.2 eV (C1s C═C), and 287.5 eV (C═O C1s), Note that the ratio of the integrated peak areas between the C═C and C═O carbons was now 18.7 : 1, almost twice the values observed with the FCA monomers and RuFCA nanoparticles (*vide ante*). This suggests that close to 50% of the surface capping ligands were decarboxylated (Scheme 1), a result consistent with the voltammetric data presented in Fig. 6. The direct attachment of the ferrocenyl moieties onto the nanoparticle surface is also manifested in ^{1}H NMR measurements with a single broad peak at around 4.3 ppm which may be assigned to the combined contributions of protons (b) and (c) whereas protons (a) were broadened into baseline (Fig. S5, ESI†). Third, for the RuFCA nanoparticles subject to the same hydrothermal treatment but without galvanic exchange reactions with Pd(II), electrochemical measurements exhibited only one pair of voltammetric peaks, essentially the same as that of the original nanoparticles. This highlights the important role of Pd in the catalytic decarboxylation of the FCA ligands on the nanoparticle surface. Fourth, no stable palladium nanoparticles could be prepared with ferrocenecarboxylate as the capping ligands by the same thermolytic route. Thus, ligand decarboxylation on monometallic Pd nanoparticles could not be tested and compared.

Conclusions

In summary, stable ruthenium nanoparticles were prepared by using ferrocenecarboxylate as protecting ligands through the formation of Ru–O bonds in a bidentate configuration, as evidenced in TEM, FTIR, ^{1}H NMR and XPS measurements. Notably, the formation of highly polarized Ru–O bonds led to a marked increase of the Fe2p binding energy as a result of the diminishment of the electron density of the ferrocenyl ring skeleton and iron center. Consistent results were obtained in electrochemical measurements where the formal potential of the particle-bound ferrocenyl moieties increased by *ca.* 120 mV as compared to that of the monomeric ligands. Importantly, the nanoparticles may undergo galvanic exchange reactions with Pd(II), leading to effective palladium-catalyzed decarboxylation of the ligands such that the ferrocenyl groups were now directly bonded to the metal surface. This was manifested in voltammetric measurements that suggested intervalence charge transfer between the ferrocenyl groups on the nanoparticle surface. The results presented herein may be of fundamental significance in the development of new protocols for the interfacial functionalization and engineering of nanoparticle materials.

Acknowledgements

This work was supported, in part, by the National Science Foundation (CHE – 1012258 and CHE – 1265635). TEM and XPS studies were carried out at the National Center for Electron Microscopy and Molecular Foundry, Lawrence Berkeley National Laboratory as part of a user project.

Notes and references

1 G. Zehl, G. Schmithals, A. Hoell, S. Haas, C. Hartnig, I. Dorbandt, P. Bogdanoff and S. Fiechter, *Angew. Chem., Int. Ed.*, 2007, **46**, 7311–7314.
2 F. Durap, M. Zahmakiran and S. Ozkar, *Int. J. Hydrogen Energy*, 2009, **34**, 7223–7230.
3 S. H. Joo, J. Y. Park, J. R. Renzas, D. R. Butcher, W. Y. Huang and G. A. Somorjai, *Nano Lett.*, 2010, **10**, 2709–2713.

4 S. W. Chen, A. C. Templeton and R. W. Murray, *Langmuir*, 2000, **16**, 3543–3548.
5 C. Pan, K. Pelzer, K. Philippot, B. Chaudret, F. Dassenoy, P. Lecante and M.-J. Casanove, *J. Am. Chem. Soc.*, 2001, **123**, 7584–7593.
6 G. Salas, C. C. Santini, K. Philippot, V. Colliere, B. Chaudret, B. Fenet and P. F. Fazzini, *Dalton Trans.*, 2011, **40**, 4660–4668.
7 W. Chen, J. R. Davies, D. Ghosh, M. C. Tong, J. P. Konopelski and S. W. Chen, *Chem. Mater.*, 2006, **18**, 5253–5259.
8 W. Chen, S. W. Chen, F. Z. Ding, H. B. Wang, L. E. Brown and J. P. Konopelski, *J. Am. Chem. Soc.*, 2008, **130**, 12156–12162.
9 W. Chen, N. B. Zuckerman, X. W. Kang, D. Ghosh, J. P. Konopelski and S. W. Chen, *J. Phys. Chem. C*, 2010, **114**, 18146–18152.
10 X. W. Kang, N. B. Zuckerman, J. P. Konopelski and S. W. Chen, *J. Am. Chem. Soc.*, 2012, **134**, 1412–1415.
11 K. Liu, X. W. Kang, Z. Y. Zhou, Y. Song, L. J. Lee, D. Tian and S. W. Chen, *J. Electroanal. Chem.*, 2013, **688**, 143–150.
12 W. Chen, N. B. Zuckerman, J. P. Konopelski and S. W. Chen, *Anal. Chem.*, 2010, **82**, 461–465.
13 X. W. Kang, N. B. Zuckerman, J. P. Konopelski and S. W. Chen, *Angew. Chem., Int. Ed.*, 2010, **49**, 9496–9499.
14 X. W. Kang, W. Chen, N. B. Zuckerman, J. P. Konopelski and S. W. Chen, *Langmuir*, 2011, **27**, 12636–12641.
15 X. W. Kang, X. Li, W. M. Hewitt, N. B. Zuckerman, J. P. Konopelski and S. W. Chen, *Anal. Chem.*, 2012, **84**, 2025–2030.
16 C. Bruneau and P. H. Dixneuf, *Ruthenium catalysts and fine chemistry*, Springer, Berlin, New York, 2004.
17 N. Chakroune, G. Viau, S. Ammar, L. Poul, D. Veautier, M. M. Chehimi, C. Mangeney, F. Villain and F. Fievet, *Langmuir*, 2005, **21**, 6788–6796.
18 N. Q. Wu, L. Fu, M. Su, M. Aslam, K. C. Wong and V. P. Dravid, *Nano Lett.*, 2004, **4**, 383–386.
19 Y. Guo, L. M. Chen, Y. Song, P. G. Hu and S. W. Chen, *Sci. Adv. Mater.*, 2014, **6**, 1060–1067.
20 D. V. Leff, L. Brandt and J. R. Heath, *Langmuir*, 1996, **12**, 4723–4730.
21 J. D. Qiu, W. M. Zhou, J. Guo, R. Wang and R. P. Liang, *Anal. Biochem.*, 2009, **385**, 264–269.
22 L. H. Guan, Z. J. Shi, M. X. Li and Z. N. Gu, *Carbon*, 2005, **43**, 2780–2785.
23 M. Yong-Xiang and M. Chun-Lin, *Chem. Pap.*, 1989, **43**, 761–770.
24 R. J. Nichols and A. Bewick, *J. Electroanal. Chem.*, 1988, **243**, 445–453.
25 G. A. Silantyev, O. A. Filippov, P. M. Tolstoy, N. V. Belkova, L. M. Epstein, K. Weisz and E. S. Shubina, *Inorg. Chem.*, 2013, **52**, 1787–1797.
26 K. Hashimoto and N. Toukai, *J. Mol. Catal. A: Chem.*, 2000, **161**, 171–178.
27 X. W. Kang and S. W. Chen, *Nanoscale*, 2012, **4**, 4183–4189.
28 R. D. Rohde, H. D. Agnew, W. S. Yeo, R. C. Bailey and J. R. Heath, *J. Am. Chem. Soc.*, 2006, **128**, 9518–9525.
29 D. R. Lide, *CRC Handbook of Chemistry and Physics*, CRC Press, Boca Raton, FL, electronic edn, 2001.
30 S. Matsubara, Y. Yokota and K. Oshima, *Org. Lett.*, 2004, **6**, 2071–2073.
31 A. C. Ribou, J. P. Launay, M. L. Sachtleben, H. Li and C. W. Spangler, *Inorg. Chem.*, 1996, **35**, 3735–3740.
32 C. Levanda, K. Bechgaard and D. O. Cowan, *J. Org. Chem.*, 1976, **41**, 2700–2704.
33 M. B. Robin and P. Day, *Adv. Inorg. Chem. Radiochem.*, 1967, **10**, 247–422.

